Conf-910651--6

To be presented at AIAA 22nd Fluid Dynamics, Plasma Dyanmids, and Laser Conference, 6/24-26/91, Honolulu, HI

A PARABOLIZED NAVIER-STOKES ANALYSIS OF WAKE/BOUNDARY-LAYER FLOW ALONG A CABLE IN TOW†

SAND--91-0878C

DE91 011497

Daniel W. Barnette‡
Computational Aerodynamics Division
Sandia National Laboratories
Albuquerque, New Mexico

Abstract

A parabolized Navier-Stokes analysis of a turbulent, compressible, wake/boundary-layer flow field for a cable in tow is discussed. It is assumed that the cable is being towed by a missile-like configuration whose total drag coefficient is known. The cable is assumed to be perfectly aligned with the missile axis and is subjected to its wake. Modeled in the analysis is the far wake behind the missile, coupled with the turbulent boundary layer growth along the cable. An analytical starting solution for a parabolized Navier-Stokes code is presented. The starting solution is applicable downstream of the towing body's near wake and, therefore, circumvents the complex task of computing the towing body's flow field. An algebraic wake/boundary-layer turbulence model is used to simulate turbulent flow in both the decaying wake and growing boundary layer along the cable. Results are presented for a towing-body freestream Mach number of 5 and a Reynolds number of 36.0×10^6 *per ft* at select distances along a thin cable.

Nomenclature

b	Wake width
B	Constant, = 5.5
C_d	Forebody total drag coefficient, based on cross section
C_{d_f}	Integrated skin friction drag coefficient, based on cross section
d	Forebody reference diameter
M	Mach number
$\overline{N}$	Surface normal, or modified surface normal
p	Pressure
P	Ratio of local density to density at edge of flat plate boundary layer
Re	Nondimensional Reynolds number
$\overline{Re}$	Reynolds number per unit length
r	Radial direction
r_0	Radius of cable or cylinder
r_0^+	Law-of-the-wall coordinate, u/v^*
T	Temperature
U, u	Streamwise velocity
u^+	Law-of-the-wall coordinate, u/v^*
v^*	Friction velocity, $\sqrt{\tau_w/\rho_w}$
w	Radial velocity
x, y, z	Axial (x) and axis-normal (y, z) Cartesian coordinates
Z	Rao's variable, κu^+

Greek

δ	Kinematic boundary layer displacement thickness
δ^*	Boundary layer height
Δ	Difference
γ	Klebanoff intermittency factor
κ	Constant, = 0.4
μ	Dynamic viscosity
ν	Kinematic viscosity
ω	Vorticity
Ω	Ratio of momentum thickness over boundary layer
ρ	Density

†This work performed at Sandia National Laboratories supported by the U.S. Department of Energy under contract No. DE-AC04-76DP00789.

‡Senior Member of Technical Staff

This paper is a work of the U.S. Government and is not subject to copyright protection in the United States.

MASTER

DISTRIBUTION OF THIS DOCUMENT IS UNLIMITED

DISCLAIMER

This report was prepared as an account of work sponsored by an agency of the United States Government. Neither the United States Government nor any agency thereof, nor any of their employees, makes any warranty, express or implied, or assumes any legal liability or responsibility for the accuracy, completeness, or usefulness of any information, apparatus, product, or process disclosed, or represents that its use would not infringe privately owned rights. Reference herein to any specific commercial product, process, or service by trade name, trademark, manufacturer, or otherwise does not necessarily constitute or imply its endorsement, recommendation, or favoring by the United States Government or any agency thereof. The views and opinions of authors expressed herein do not necessarily state or reflect those of the United States Government or any agency thereof.

DISCLAIMER

Portions of this document may be illegible in electronic image products. Images are produced from the best available original document.

τ	Shear stress

Subscripts

bl	Boundary layer
cl	Centerline
e	Edge conditions
i	Incompressible, inner
max	Maximum
o	Outer
pl	Flat plate
t	Turbulent
w	Wake, wall value
∞	Freestream conditions

Superscripts

n	An arbitrary exponent
$+$	Law-of-the-wall coordinate

Introduction

The objective of the current analysis is to determine the drag of a cable in tow and subjected to a compressible, turbulent, high Reynolds-number, wake/boundary-layer flow. The cable is assumed to be in tow behind a missile-like configuration at zero angle of attack and perfectly aligned with the missile axis. The entire length of the cable is subjected to the missile's wake. The diameter of the cable is assumed small relative to the towing body diameter. Such an analysis is applicable, for example, to an antenna protruding from a base of a missile or reentry vehicle.

It is well known that flow field properties at the edge of a far wake flow field are constant. Pressure across the wake is typically assumed to be constant as well. These assumptions are identical to those made for flat-plate boundary layer flow. A cable in tow, immersed in a wake, generates an axial boundary layer that grows subject to edge conditions imposed by the wake. The growth of the towing-body wake and cable boundary layer are inherently coupled. It is intuitive that, although coupled, a wake with an embedded boundary layer would retain a boundary-layer-like nature.

A suitable computational approach to determining cable drag is appropriate since analytical expressions, wind tunnel data, flight test data, or other computational analyses are not known to exist for this type of flow field. Widely-used parabolized Navier-Stokes (PNS) codes offer an accurate, efficient solution method for high-speed, boundary-layer type flows. PNS codes solve the three-dimensional or axisymmetric, steady, Navier-Stokes equations using a spatial marching algorithm. Formulation of the PNS equations disallows regions of reverse flow. These codes require a starting solution as an initial condition to marching the governing equations. It is plausible that, given suitable initial conditions, a PNS analysis is possible for the wake/boundary-layer flow on the cable.

A straight-forward method of obtaining suitable PNS initial conditions on the cable is to first solve the flow field over the towing body. This would require Navier-Stokes solutions over at least a portion of the towing body, most notably the base. This is a time-consuming, compute-intensive process. A significant savings in time and resources can be realized by developing an analytical starting solution aft of the towing body that couples both the wake and the cable boundary layer. For a PNS analysis to be applicable, the starting solution must be valid downstream of the recirculating base flow region.

Presented below is the development of an analytical starting solution applicable for a PNS code for the turbulent wake/boundary-layer flow along a cable. The starting solution was formed by computing and merging calculated wake and cable boundary layer profiles aft of the towing body near wake. Knowledge of the towing-body drag coefficient and reference diameter allows determination of a wake/boundary-layer velocity profile on the cable, as will be discussed.

Development of a wake/boundary-layer turbulence model is also discussed since the flow was assumed turbulent. The standard two-layer, algebraic Cebeci-Smith turbulence model was modified to account for length scales appropriate for the wake and for compressibility effects. The model also accounts for transverse curvature effects which occur when the boundary layer height becomes large relative to the diameter of the cable.

Sandia's parabolized Navier-Stokes (PNS) code SPRINT[1-3] was used to compute the flow field. SPRINT is an extensively modified descendant of the Air Force Wright Aeronautical Laboratories' PNS code.[4,5] Results are presented for sea level flight conditions of the towing body at Mach 5 and a Reynolds number of 36.0×10^6 *per ft*. A constant, specified temperature of $T_w = 540^\circ R$ was enforced along the cable. Freestream temperature was $T_\infty = 540^\circ R$. The total drag coefficient and reference diameter of the towing vehicle are

$C_d = 0.30$ and $d = 1.00$ *in*, respectively. The cable is assumed to be perfectly smooth and rigid. Cable diameter is 0.040 *in*.

Development of the PNS Starting Solution

The development of a PNS starting solution begins by considering the physics of wake flow and boundary layer flow on a cable, then merging these flow fields in a physically valid manner. It should be emphasized that merging of the wake/boundary-layer flow was the approach used only for patching together the initial conditions for the PNS code. While marching downstream of the starting location, the numerical solution automatically accounts for the influence these two flow fields have on each other and on the freestream.

First, consider the wake behind a vehicle with a flat base flying at supersonic speed. A wake in high-Reynolds number flow can be divided into three regions: near wake (or recirculation) region, neck (or transitional) region, and far wake (or viscous wake) region. Fig. 1 illustrates fundamentals of wake flow in a supersonic stream. Alber and Lees[6] describe the near wake behind a step in detail, for both laminar and turbulent approaching boundary layers. This flow is depicted in Fig. 1a. The extent of the recirculation region, *i.e.*, the distance from the base to the rear stagnation point, is longer for low Mach numbers. Extent of the near wake has been found to be less than $5 - 10$ body diameters downstream of the base.[6–9]

The far wake illustrated in Fig. 1b commences several body diameters downstream of the point where the wake shock emerges from the viscous wake. The far wake can commence at axial distances of $x/d = 5$ or more, as measured from the base of the vehicle.[7] The distinct lip and wake shocks, obvious in the near wake and transitional region, have coalesced and are collectively referred to as the wake shock. Flow field properties at the edge of the wake are constant, as is the pressure across the wake.[8] Hence, $\partial p/\partial y = 0$ across the wake. These assumptions are identical to those made for flat-plate boundary layer flow. Hence, similarity profiles prevail in the far wake. By the term "similarity" is meant that the wake velocity profiles become similar in shape when normalized by variables or parameters characteristic of the flow field. The characteristic variables for a wake are its local centerline velocity and width. The existence of similarity will prove to be extremely useful in the analysis that follows.

Next, consider only the boundary layer flow along a cable or cylinder in the axial direction. Boundary layer growth is dependent on the edge Reynolds number. The edge Reynolds number is typically computed by determining the boundary layer height to be $95 - 99\%$ of the height from the wall or surface to where freestream, or edge, conditions prevail. For a long cable, the boundary layer height can grow so large that transverse curvature effects significantly alter what might otherwise be a Blasius profile.

Finally, consider the merging of a wake and a boundary layer. Typically, the displacement thickness due to the boundary layer would displace the wake outward by the same amount. For the current analysis, it is desirable to merge the flow fields very near (but downstream of) the stagnation point associated with the near wake. The diameter of the cable is assumed small compared to the wake diameter near this region. It may then be hypothesized that the boundary layer displacement thickness induces a higher-order effect on the wake flow which can be ignored in the development of a PNS starting solution. On the other hand, the effect of the wake flow on the boundary layer is significant since edge conditions for the boundary layer are found within the velocity profile of the wake. The velocity defect associated with the wake is greatest near the near-wake stagnation point. Hence, its effect on the boundary layer must be accounted for.

Listed in Table 1 are incompressible laminar and turbulent growth rates for an axisymmetric boundary layer (assuming the boundary layer height is much smaller than the cylinder diameter), an axisymmetric wake, a flat plate boundary layer, and a plane two-dimensional wake. The author was unable to find growth rates for an axisymmetric boundary layer which is large relative to cylinder diameter. Note that for turbulent flow, the growth rates for the axisymmetric and flat plate boundary layer (both $x^{4/5}$) are greater than the axisymmetric wake ($x^{1/3}$) and the plane two-dimensional wake ($x^{1/2}$). Hence, it is expected that the boundary layer of the merged wake/boundary-layer flow field will grow at a rate faster than the wake and become the dominant feature far downstream of the towing vehicle. As will be seen, the computations have indicated this to be the case.

The methods used in generating the forward-body wake profile, cable boundary-layer profile, and the merged wake/boundary-layer profile for the SPRINT starting solution are discussed below.

Forebody Wake Profile

No analysis could be found representing compressible velocity profiles across the wake. Hence, the fol-

	laminar	turbulent
Axisymmetric b.l. ($\delta \ll r_0$)	$x^{1/2}$	$x^{4/5}$
Axisymmetric wake	$x^{1/2}$	$x^{1/3}$
Flat Plate Boundary Layer	$x^{1/2}$	$x^{4/5}$
Plane 2-D Wake	$x^{1/2}$	$x^{1/2}$

Table 1: Laminar and turbulent power laws for streamwise growth of incompressible boundary layers and wakes.

lowing development incorporates an incompressible wake profile which will be used as part of a starting solution for SPRINT, a compressible flow field code. Perturbations arising from this compressibility mismatch quickly dampen as SPRINT is marched along the cable, as will be discussed.

Assume that velocity profiles in the far wake region are similar, that the turbulent mixing length is proportional to the wake width $b(x)$ (after Prandtl), and that the momentum defect associated with the wake profile remains constant far downstream. Then the velocity defect profile for a turbulent, incompressible, axisymmetric wake is given by

$$\frac{u}{U_{e,w}} = 1 - \frac{\Delta u_{max}}{U_{e,w}} \left[1 - \left(\frac{r}{b(x)} \right)^{3/2} \right]^2 . \quad (1)$$

where $\Delta u_{max} = U_{e,w} - U_{cl}$.[10] Using an analysis similar to that discussed in Ref. 8 for a plane wake, it can be shown that the velocity defect along the centerline of an axisymmetric wake is given by the expression

$$\frac{\Delta u_{max}}{U_{e,w}} = \frac{70}{288} \left(\frac{d}{b(x)} \right)^2 C_d . \quad (2)$$

From Lyons, *et al*,[11] the width of the turbulent far wake behind cones flying at Mach numbers of from 5.0 to 7.7 can be correlated by the expression

$$\frac{b(x)}{d} = \frac{0.7}{2} \left(C_d \frac{x}{d} \right)^{1/3} \quad (3)$$

where x is measured from the base of the vehicle. Hence, the decay of the centerline velocity can be expressed by

$$\frac{\Delta u_{max}}{U_{e,w}} = \frac{70}{288} \left(\frac{2}{0.7} \right)^2 \left(\frac{C_d^{1/2} d}{x} \right)^{2/3} . \quad (4)$$

The continuity equation in cylindrical coordinates can be used together with Eqs. 1 and 2 to give the w velocity profile in the radial, or r, direction. Hence, the axial and radial velocity profiles for an incompressible, turbulent, axisymmetric wake are given by

$$\frac{u}{U_{e,w}} = 1 - \frac{70}{288} \left(\frac{2}{0.7} \right)^2 \left(\frac{C_d^{1/2} d}{x} \right)^{2/3} \left[1 - \left(\frac{r}{b(x)} \right)^{3/2} \right]^2 \quad (5)$$

$$\frac{w}{U_{e,w}} = -\frac{2}{0.7} \left(\frac{C_d^{1/2} d}{x} \right)^{4/3} \left[\frac{1}{5} \left(\frac{r}{b(x)} \right)^4 - \frac{2}{7} \left(\frac{r}{b(x)} \right)^{5/2} + \frac{3}{35} \left(\frac{b(x)}{r} \right) \right] . \quad (6)$$

As expected, the negative sign on the last equation indicates that the radial flow of a wake is inward, *i.e.*, towards the centerline.

The above equations will be collectively referred to as the "Lyons-Prandtl wake velocity profile."

Cable Boundary Layer Profile

Assume that a turbulent boundary layer profile can be predicted by the well-known power law

$$\frac{u}{u_e} = \left(\frac{y}{\delta} \right)^{\frac{1}{n}} . \quad (7)$$

For turbulent profiles, n is typically taken to be 7 or 9. Eckert[12,13] showed that the compressible boundary layer height for axial flow along a cylinder (or cable) is given implicitly by

$$\frac{\delta}{\delta_{pl}} = \left(1 + \frac{n+3}{2n+4} \frac{\Omega_{2n}}{\Omega_n} \frac{\delta}{r_0} \right)^{-\frac{(n+1)}{(n+3)}} . \quad (8)$$

Here, δ is the boundary layer thickness on the cylinder and δ_{pl} is the flat plate boundary layer height at the same Reynolds number, $U_e x/\nu_e$, as for δ. The function Ω represents the ratio of momentum thickness for the flat plate over δ_{pl} and is given by the expression

$$\Omega_n = \frac{n}{n+1} P_{n+1} - \frac{n}{n+2} P_{n+2} \quad (9)$$

$$P_n = \int_0^1 \frac{d\left(\frac{y}{\delta}\right)}{1 + \frac{\gamma-1}{2} M_e^2 \left[1 - \left(\frac{y}{\delta} \right)^{2/n} \right]} . \quad (10)$$

$P_n = \rho/\rho_e$, the ratio of the local density to the density at the boundary layer edge for the flat plate. The compressible boundary layer height for a flat plate, ratioed to the incompressible height, is given by

$$\frac{\delta_{pl}}{\delta_i} = \left(\frac{\Omega_i}{\Omega_n}\right)^{4/5} \left(\frac{\overline{T}}{T_e}\right)^{-11/25} \tag{11}$$

where

$$\Omega_i = \frac{n}{(n+2)(n+1)} , \tag{12}$$

$$\delta_i = 0.381 x Re^{-1/5} , \tag{13}$$

$$\frac{\overline{T}}{T_e} = P_{n+1}^{-1} . \tag{14}$$

Hence, δ_{pl} can be calculated from the expression

$$\delta_{pl} = \frac{\delta_{pl}}{\delta_i}\delta_i . \tag{15}$$

Once the boundary layer thickness on the cable or cylinder is determined from Eq. 8, a suitable boundary layer velocity profile must be calculated. The profile should account for boundary layer thicknesses on the order of the radius of the cylinder, in which case tranverse curvature effects become important. Hence, a more general expression than that given by Eq. 7 is needed, even though that equation was used to determine boundary layer thickness. An appropriate expression can be found in Rao's modification of Spalding's composite formula for the inner law of the wall and the logarithmic overlap region of the boundary layer.[14] Rao's modification leads to the equation

$$r_0^+ \ln \frac{r}{r_0} = u^+ + e^{-\kappa B}\left(e^Z - 1 - Z - \frac{1}{2}Z^2 - \frac{1}{6}Z^3\right) \tag{16}$$

which must be solved implicitly for u.

The "w," or radial, velocity will not be considered in the formulation of the cable boundary layer profile for the starting solution. There are several reasons for this. First, the boundary layer influence is extremely small immediately downstream of the near-wake stagnation point. Second, the flow in this region is mainly wake dominated, and the radial velocity component has been included in the wake formulation. Third, the finite difference equations in SPRINT do account for the "w" velocity term and will very quickly generate this velocity as the equations are marched along the cable. Fourth, any perturbations introduced into the marching solution due to the initially-missing velocity are expected to quickly damp. For these reasons, ignoring this radial velocity component in the comparatively small boundary layer did not hinder generating a valid starting solution.

Eqs. 8 and 16 will be collectively referred to as the "Eckert-Rao boundary layer profile."

Merged Wake/Boundary-Layer Profile

The Eckert-Rao boundary layer profile and the Lyons-Prandtl wake profile must be merged to generate a starting solution to the SPRINT code, assuming no-slip conditions at the wall. The merged starting solution will then simulate axial, viscous flow of a wake at a specified location along the cable. The starting solution must be generated close to the near wake to computationally couple the wake and boundary layer as soon as possible. This is also desirable from the standpoint of allowing numerical perturbations arising from the starting profile to damp as far upstream as possible.

The boundary layer height in the wake is determined *via* an iterative process, as follows. First, the freestream velocity is used to determine the edge Reynolds number with which the boundary layer edge is calculated from the Eckert-Rao boundary layer profile. The wake velocity at this boundary layer edge location is calculated from the Lyons-Prandtl wake profile. This velocity is then used to calculate the new location of the edge of the boundary layer, and the process is repeated. This method converges very quickly, typically with little or no change in results after approximately five iterations. A short computer code was written to perform the necessary iterations and format the output for use in starting the SPRINT code.

All results were obtained from sea level flight conditions of the towing body at Mach 5 and a Reynolds number of 36.0×10^6 *per ft*. It is assumed that pressure and density are constant across the wake/boundary-layer for the starting solution. A constant, specified temperature of $T_w = 580°R$ was enforced along the cable. Freestream conditions were enforced at the top of the wake. Freestream temperature was $T_\infty = 540°R$. Imposing freestream boundary conditions at the edge of the wake is an approximation based on the assumption that the "far-field" flow aft of the towing vehicle has returned to essentially freestream conditions.

With the wake/boundary-layer velocities, pressure, density, and boundary conditions thus specified, the starting solution for SPRINT is completely specified.

Wake/Boundary-Layer Turbulence Model

Turbulent boundary layer and wake flow is assumed along the cable. The development of a wake/boundary-layer turbulence model must account for turbulence both in the wake and in the boundary layer. The SPRINT code contains variations of two algebraic, two-layer, eddy viscosity turbulence models: that of Baldwin-Lomax[15] and of Cebeci-Smith[16]. These models allow determination of the turbulent eddy viscosity by dividing the boundary layer into two layers, an "inner" and an "outer" region.

Preliminary solutions were obtained using the Baldwin-Lomax turbulence model. This model introduced significant, non-physical perturbations into the axial pressure distribution along the cable. Reasons for this behavior have been documented[17,18] and pertain to the differential form of the outer eddy viscosity model. Hence, the Baldwin-Lomax model was replaced by the Cebeci-Smith model for the results presented herein. The latter model uses an integral form for the outer eddy viscosity which acts to smooth perturbations. The previously-observed perturbations were not observed using the Cebeci-Smith model for the present calculations.

In this work, a modified form of the two-layer Cebeci-Smith model was developed to account for wake/boundary-layer turbulence. The inner eddy viscosity model is that of Cebeci-Smith, modified to account for the possibility of transverse curvature effects. Modifications were also made to the outer eddy viscosity model to account for wake turbulence and the possibility that the cable boundary layer might become large enough to dominate the wake flow. As was shown in Table 1, the boundary layer thickness increases faster than that of the wake width for axisymmetric turbulent flows with small boundary layers. Hence, the outer eddy viscosity model for the wake becomes invalid should the boundary layer thickness approach the wake width. When this occurs, the standard form of the Cebeci-Smith outer eddy viscosity model supercedes the wake outer eddy viscosity model.

Details of the wake/boundary-layer turbulence model are as follows. For thin boundary layers ($\delta_{bl} \ll r_0$), the expression for the inner eddy viscosity is given by

$$(\mu_t)_i = \rho \overline{Re}_\infty \omega \left\{ 0.4 \overline{N} \left[1 - \exp\left(-\frac{1}{26} \sqrt{\frac{\overline{Re}_\infty \rho_w \omega_w}{\mu_w}} \sqrt{\frac{\rho}{\rho_w}} \frac{\mu_w}{\mu} \overline{N} \right) \right] \right\}^2 \quad (17)$$

Square brackets enclose the compressible form of the Van Driest damping term. Transverse curvature effects for $\delta_{bl} \simeq r_0$ are accounted for in the above equation by two modifications.[16] First, the substitute expression

$$\overline{N} = r_0 \ln\left(\frac{r}{r_0}\right) \quad (18)$$

is used. Second, the entire right hand side of Eq. 17 is multiplied by the quantity r/r_0.

An outer eddy viscosity model for the wake is developed in a form analagous to that deduced by White[10] for jets. His assumption is that the eddy viscosity for jets must be scaled by the jet centerline (maximum) velocity and the jet width. The analagous form for wakes is that the eddy viscosity must be scaled by the velocity defect, Δu_{max}, and the wake width, $b(x)$. When a boundary layer exists in the core of the wake due to axial flow along a cylinder, as shown in Fig. 2, the modified wake width is then given approximately by the expression

$$b'(x) = b(x) + 2\left(\delta^* + r_0 - \delta\right) . \quad (19)$$

where the kinematic displacement thickness δ^* for flow past an axisymmetric body of radius r_0 is given by

$$\delta^* = -r_0 + \left[(\delta + r_0)^2 - 2 \int_{r_0}^{\delta + r_0} \left(\frac{u}{U_{e,bl}} \right) r dr \right]^{1/2} . \quad (20)$$

Eq. 20 is derived by noting that the width of the wake alone will be displaced by the physical presence of the cable and its boundary layer displacement thickness. Hence, the wake outer eddy viscosity model, which assumes the existence of a boundary layer in the wake's core, is given by

$$(\mu_t)_{o,w} = 0.0168 \overline{Re}_\infty \rho \Delta u_{max} b' \gamma_w \quad (21)$$

where the Klebanoff intermittency factor for the wake, γ_w, is given by

$$\gamma_w = \left[1 + 5.5 \left(\frac{\overline{N} - \delta}{b'} \right)^6 \right]^{-1} . \quad (22)$$

As has been discussed, growth of the boundary layer height is faster than growth of the wake width. Hence, it is possible for the eddy viscosity of the boundary layer to be higher than that of the wake's for long cable lengths. In this case, the standard form of the Cebeci-Smith outer eddy viscosity model is used and is given by the equation

$$(\mu_t)_{o,bl} = 0.0168\overline{Re}_\infty \rho U_{e,bl} \delta^* \gamma_{bl} \qquad (23)$$

where $U_{e,bl}$ represents the velocity at the edge of the boundary layer. The intermittency factor for the boundary layer, γ_{bl}, is given by

$$\gamma_{bl} = \left[1 + 5.5\left(\frac{\overline{N}}{\delta}\right)^6\right]^{-1} . \qquad (24)$$

The outer eddy viscosity for the merged wake/boundary-layer flow field is chosen from the largest value calculated from Eq. 21 or Eq. 23.

Boundary layer height for the wake/boundary-layer turbulence model is determined using the starting solution iterative procedure discussed previously. The only difference is that the numerically-determined velocity profile (instead of Rao's modification, Eq. 16) is used in Eckert's equation, Eq. 8. Also, the local displacement thickness, Eq. 20, is added to the wake thickness, Eq. 3, to get the corrected wake thickness.

Computational Comparisons and Results

To the author's knowledge, no flight, experimental, or other computational results are known to exist for a long cable in tow. This precludes direct, independent verification of the present computational results. However, some manner of validation of the present analysis was felt necessary. Two efforts were undertaken to at least provide information as to whether the computed profiles were intuitively correct.

The first validation effort involved comparing the analytical Eckert-Rao boundary layer profiles with computational results from the SPRINT code for freestream (no wake) edge conditions. The purpose in this effort was to gain confidence in the accuracy of the Eckert-Rao profiles. For this case, the cable was assumed to have a 9.46 *deg* conical tip. A conical step-back procedure was used to generate a starting solution for SPRINT. Results are presented in Fig. 3 for $x = 15.0$ *in* and $x = 50.0$ *in*. Agreement is seen to be very good. Also, the calculated boundary layer thickness was found to be relatively insensitive to the velocity profile exponent "n". For example, the boundary layer height 15 *in* along the cable was calculated to be 0.1056 *in* for $n = 7$ and .1094 *in* for $n = 12$. At 50 *in*, the results also compared favorably at 0.1929 *in* for $n = 7$ and 0.2000 *in* for $n = 12$. These comparisons validate the use of the Eckert-Rao boundary layer profile in constructing the boundary layer region of the wake/boundary-layer starting solution for SPRINT.

The second validation effort involved comparing Lyons-Prandtl wake profiles (no cable) with computed wake/boundary-layer profiles and the computed boundary layer profiles (no wake) from above, at select cable locations. The purpose in this effort was to gain confidence in the accuracy of the Lyons-Prandtl profiles. The wake/boundary-layer solutions and cable boundary layer profiles (no wake) were computed using SPRINT. The starting solution for the wake/boundary-layer solutions was formed at a point along the cable 15.00 *in* from the base of the towing body, downstream of the near wake. The solution was input to the SPRINT code which was marched to the 38.34 *in* station. Fig. 4 indicates the amplitude of the initial oscillation is relatively large but damps within 5 *in* (5 base radii). Similar behavior was observed when the solution was started at a point 30.00 *in* from the base. An extremely low value of artificial viscosity ($\epsilon_e = 0.005$ in SPRINT) was used so as not to significantly influence the solution once the oscillations damped. Large values of smoothing would decrease the amplitude of the oscillations but might significantly influence the solution farther downstream. The oscillations occur for several possible reasons. One reason is that the merged wake/boundary-layer profile used in the starting solution was developed using incompressible wake relations. Another is that the radial velocity is not considered in the formulation of the initial cable boundary layer profile. Still another is that the influence of the wake on the cable boundary layer is taken into account *via* the boundary layer's edge velocity but the effect of boundary layer displacement thickness on the wake is initially ignored.

Presented in Fig. 5 are velocity profile comparisons for the forebody wake, cable boundary layer, and wake/boundary-layer at various distances along the cable. For correct comparisons, cable length for the boundary layer calculations should be measured from the near-wake stagnation point since this is where the boundary layer originates in the wake/boundary-layer flow. Since this point is unknown and the extent of the near-wake stagnation region is assumed small relative to the cable lengths, cable boundary layer calculations are measured from the base of the towing body. In each case, the wake/boundary-layer profile is higher than either the wake or boundary layer profile at that location. This is expected since the displacement thickness of the boundary layer also acts to displace the wake width. The figures show that the near-wall profile of the wake/boundary-layer lies between the wake profile and

Cable length (*inches*)	C_{d_f}, no wake	C_{d_f}, in wake
38.37	0.0123	0.0048
77.74	0.0248	0.0147
117.11	0.0373	0.0252
156.48	0.0497	0.0361
235.22	0.0744	0.0582

Table 2: Integrated skin friction coefficient data for various cable lengths.

the cable boundary layer. This is also expected since the wake velocity profile has a mitigating effect on the boundary layer (no wake) velocity profile. Further examination shows that boundary layer growth occurs faster than wake growth. Far downstream, the boundary layer will dominate the wake. This conclusion was inferred from the incompressible wake and boundary layer growth rates presented in Table 1.

Presented in Fig. 6 are wake/boundary-layer profiles of local quantities at select distances along the cable. Presented in Fig. 6a is the local Mach number u/a and the density ρ/ρ_∞ in Fig. 6b. It is apparent that the wake effects have diminished at the longer cable length. The flow becomes dominated by the large boundary layer. Note the steep density gradients near the wall due to the specified temperature of the cable in Fig. 6b.

The cable integrated skin friction drag coefficient C_{d_f} is presented in Fig. 7 as a function of cable length. The numerical data are presented in Table 2. Results for the "cable alone, no wake" (no towing body) and "cable alone, in wake" (behind towing body) are compared. As expected, the effect of the wake is to reduce the drag on the cable. In this case, a drag reduction of approximately 20% is observed at the longest cable length.

Summary and Conclusions

An efficient computational method using a parabolized Navier-Stokes code has been developed to determine the wake/boundary-layer flow field along a cable in tow. Total drag and reference diameter of the towing body are assumed known. An analytical starting solution developed for the PNS code has been presented. The starting solution was used to initialize computations immediately aft of the near wake of the towing body. A wake/boundary-layer turbulence model has also been developed to model wake decay and boundary layer growth along the cable. These developments were used to determine the flow field and aerodynamic drag along the cable. No wind tunnel data, flight test data, analytical solutions, or other computational analyses are known to exist for long cables in tow. Computational comparisons indicate that the methods used to generate turbulent wake/boundary-layer profiles are valid. These methods offer the computational analyst a significant savings in time and resources by circumventing the compute-intensive task of solving the flow field over the towing body.

Acknowledgments

The author would like to express appreciation to Sandia National Laboratories' F. G. Blottner, Senior Member Technical Staff, Computational Aerodynamics Division, and W. L. Oberkampf, Supervisor, Computational Aerodynamics Division, for the many helpful discussions regarding numerical simulations of wake/boundary-layer flow.

References

1. M. A. Walker, "SPRINTRUN: A User-Friendly Input Processor for the SPRINT Code," SAND89-0625, Sandia National Laboratories, Albuquerque, New Mexico, March 1990.

2. M. McWherter, R. W. Noack, and W. L. Oberkampf, "Evaluation of Boundary-Layer and Parabolized Navier-Stokes Solutions for Re-entry Vehicles," *Journal of Spacecraft and Rockets*, Vol. 23, No. 1, January-February 1986, pp. 70-78.

3. M. McWherter and W. L. Oberkampf, "Force and Moment Computations Using the AFWAL Parabolized Navier-Stokes Code," SAND87-0470, Sandia National Laboratories, Albuquerque, New Mexico, March 1985.

4. J. F. Stalnaker, L. A. Nicholson, D. S. Hanline, and E. H. McGraw, "Improvements to the AFWAL Parabolized Navier-Stokes Code Formulation," AFWAL-TR-86-3076, September 1986.

5. S. P. Shanks, G. R. Srinivasan, and W. E. Nicolet, "AFWAL Parabolized Navier-Stokes Code: Formulation and User's Manual," AFWAL-TR-82-3034, June 1982.

6. I. E. Alber and L. Lees, "Integral Theory for Supersonic Turbulent Base Flows," *AIAA Journal*, Vol. 6, No. 7, July 1968, pp. 1343-1351.

7. D. K. McLaughlin, J. E. Carter, M. Finston, and J. A. Forney, "Experimental Investigation of the Mean Flow of the Laminar Supersonic Cone Wake," *AIAA Journal*, Vol. 9, No. 3, March 1971, pp. 479-484.

8. A. Martellucci, H. Trucco, and A. Agnone, "Measurements of the Turbulent Near Wake of a Cone at Mach 6," *AIAA Journal*, Vol. 4, No. 3, March 1966, pp. 385-391.

9. E. M. Murman, "Experimental Studies of a Laminar Hypersonic Cone Wake," *AIAA Journal*, Vol. 7, No. 9, September 1969, pp. 1724-1730.

10. F. M. White, Viscous Fluid Flow, McGraw-Hill Book Company, 1974.

11. W. C. Lyons, J. J. Brady, and Z. J. Levensteins, "Hypersonic Drag, Stability, and Wake Data for Cones and Spheres," *AIAA Journal*, Vol. 2, No. 11, November 1964, pp. 1948-1956.

12. H. U. Eckert, "Characteristics of the Turbulent Boundary Layer on a Flat Plate in Compressible Flow from Measurements of Friction in Pipes," *Journal of the Aeronautical Sciences*, Vol. 17, September 1950, pp. 573-584.

13. H. U. Eckert, "Simplified Treatment of the Turbulent Boundary Layer Along a Cylinder in Compressible Flow," *Journal of the Aeronautical Sciences*, Vol. 19, January 1952, pp. 23-28.

14. G. N. V. Rao, "The Law of the Wall in a Thick Axisymmetric Turbulent Boundary Layer," *Journal of Applied Mechanics*, March 1967, pp. 237-238.

15. B. Baldwin and H. Lomax, "Thin Layer Approximation and Algebraic Model for Separated Turbulent Flows," AIAA Paper 78-257, presented at the AIAA 16th Aerospace Sciences Meeting, Huntsville, Alabama, January 1978.

16. T. Cebeci and A. M. O. Smith, Analysis of Turbulent Boundary Layers," Academic Press, 1974.

17. S. A. Shirazi and C. R. Truman, "Evaluation of Algebraic Turbulence Models for PNS Predictions of Supersonic Flow Past a Sphere-Cone," *AIAA Journal*, Vol. 27, No. 5, May 1989, pp. 560-568.

18. _____, "Simple Turbulence Models for Supersonic and Hypersonic Flows: Bodies at Incidence and Compression Corners," presented as AIAA Paper 89-0669, 27th Aerospace Sciences Meeting, Reno, Nevada, January 1989.

DISCLAIMER

This report was prepared as an account of work sponsored by an agency of the United States Government. Neither the United States Government nor any agency thereof, nor any of their employees, makes any warranty, express or implied, or assumes any legal liability or responsibility for the accuracy, completeness, or usefulness of any information, apparatus, product, or process disclosed, or represents that its use would not infringe privately owned rights. Reference herein to any specific commercial product, process, or service by trade name, trademark, manufacturer, or otherwise does not necessarily constitute or imply its endorsement, recommendation, or favoring by the United States Government or any agency thereof. The views and opinions of authors expressed herein do not necessarily state or reflect those of the United States Government or any agency thereof.

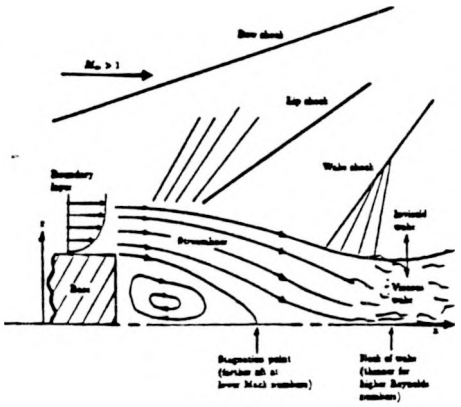

a) Near-wake flow

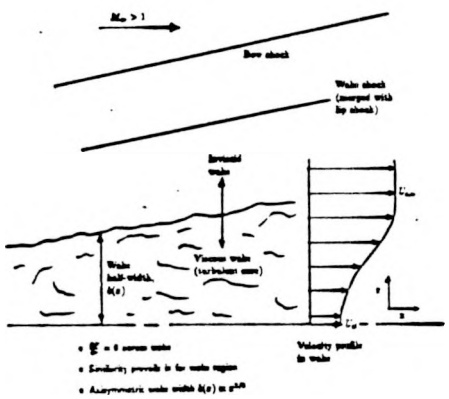

b) Far-wake flow

Figure 1: Fundamental aspects of high Reynolds number, turbulent, supersonic wake flow.

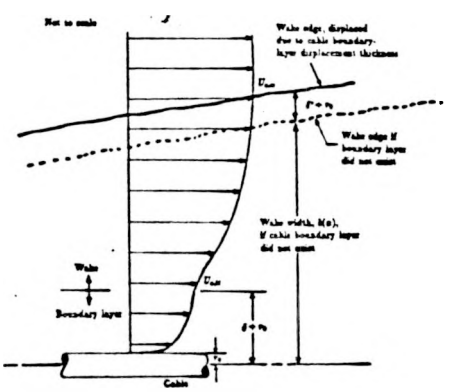

Figure 2: Sketch of wake/boundary-layer profile illustrating length scales.

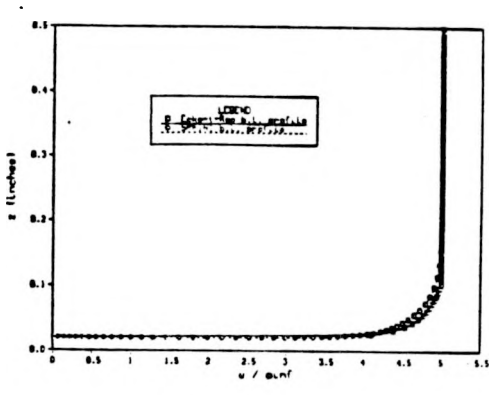

a) x = 15 *in*

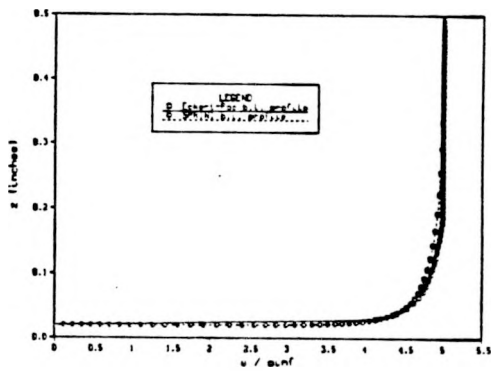

b) x = 50 *in*

Figure 3: Comparison of boundary layer profiles for Mach 5 axial flow over a cable ($r_0 = 0.020$ *in*; Reynolds number = 36.0×10^6 *per ft*).

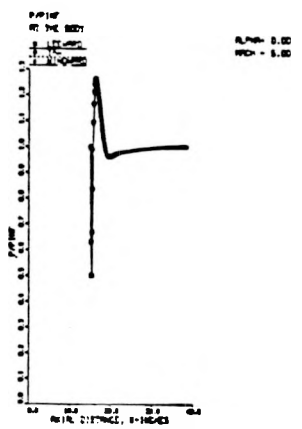

Figure 4: Pressure ratio p/p_∞ as a function of distance along the cable.

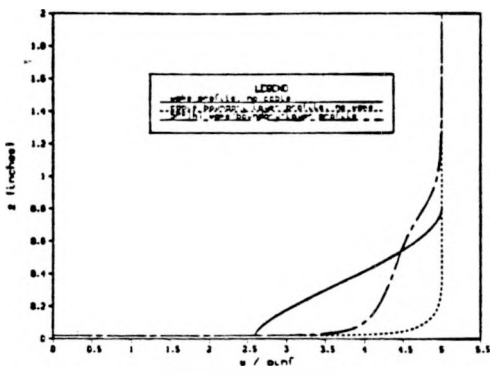

a) x = 38.34 *in*

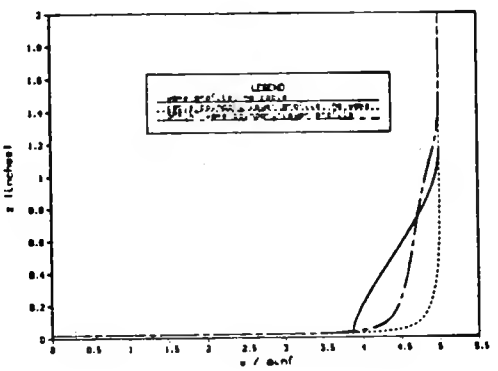

b) x = 117.11 *in*

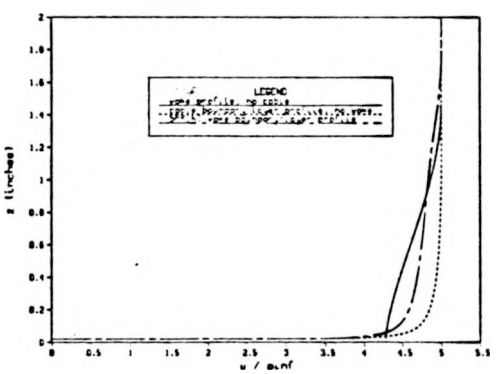

c) x = 235.22 *in*

Figure 5: Profiles of forebody wake, cable boundary layer, and wake/boundary layer.

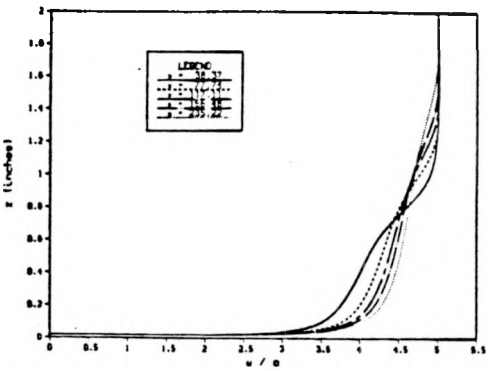

a) Local Mach number

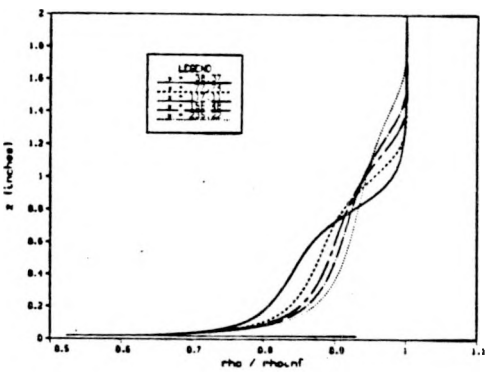

b) Density

Figure 6: Wake/boundary-layer profiles at select distances along the cable.

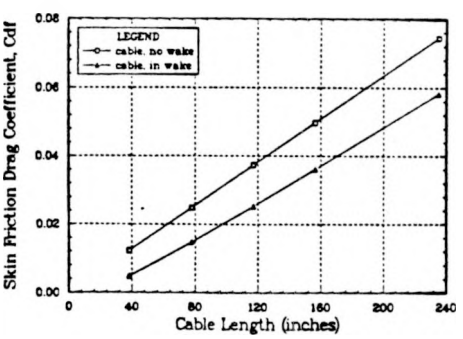

Figure 7: Integrated skin friction drag coefficient *vs.* cable length illustrating wake effects.